

Continuous-time control of alternans in long Purkinje fibers

Alejandro Garzón,^{1, a)} Roman O. Grigoriev,² and Flavio H. Fenton²

¹⁾*School of Exact Sciences and Engineering, Universidad Sergio Arboleda, Bogota, Colombia*

²⁾*School of Physics, Georgia Institute of Technology, Atlanta, Georgia 30332-0430, USA*

(Dated: 8 April 2014)

Alternans – an arrhythmic response of cardiac tissue to periodic pacing – often serves as a precursor to a more dangerous, and potentially lethal, state of fibrillation. Suppression of alternans using feedback control may be a plausible method to prevent fibrillation. Several approaches based on impulsive control have been proposed previously, where feedback is applied for a brief instance of time during each pacing interval. This paper presents a continuous-time approach, where feedback current is applied at all times, which is capable of suppressing alternans in fibers of significantly greater length (up to at least 4 cm), compared with impulsive control (less than 1 cm), and for a wide range of pacing cycle lengths.

Control of cardiac arrhythmias, from dangerous (such as atrial tachycardia) to deadly (such as ventricular fibrillation), is a problem of great medical importance. While drug therapies and tissue ablations are often successful in treating atrial arrhythmias¹, implantable cardioverter-defibrillators (ICDs) are usually required to terminate the more deadly arrhythmias in the ventricles. Currently ICDs employ up to three leads for continuous monitoring and, if arrhythmia is detected, for suppressing it using several modes: pacing, fast pacing (anti-tachycardia pacing), high energy shocks (cardioversion), or very high energy shocks (defibrillation). However, despite the many improvements in our fundamental understanding of arrhythmic dynamics and mechanisms of defibrillation²⁻⁶, there is still a lot of room for improving the control algorithms. In particular, using model-based feedback control would allow the ICDs to suppress arrhythmias using much weaker electrical currents thus avoiding pain and tissue damage. This paper explores the limits of spatially localized feedback control by focusing on one of the simplest active components of the heart – the Purkinje fibers. These are strands of tissue that transmit the excitation waves from the atria to the ventricles, initiating their contraction. While Purkinje fibers are effectively one-dimensional, as opposed to the atrial and ventricular tissue, which are effectively two- or three-dimensional, they exhibit the same fundamental mode of period doubling instability (known as alternans), thus allowing us to understand in a simpler model the interplay between the action of the feedback and the information flow associated with the nonlinear waves propagating through the tissue. Achieving full con-

trol of a relatively simple system such as a Purkinje fiber is one of the first steps in developing improved feedback control algorithms for other types of cardiac tissue and, eventually the entire organ.

I. INTRODUCTION

The contraction of the heart is controlled by an electrochemical excitation wave, with the sinoatrial node serving as the pacemaker. Normal rhythm is characterized by a wave propagating over the entire heart in a highly coordinated way. Occasionally, the heart can transition to a lethal arrhythmic behavior known as ventricular fibrillation (VF) characterized by turbulent dynamics^{5,7} lacking spatial coordination which renders the heart incapable of pumping blood. The first step in the transition from normal rhythm to VF is often associated with a periodic alternation in the duration of the electrical excitation from beat to beat, known as electrical alternans^{8,9}. It makes sense then to assume that suppression of alternans, which leads to stabilization of normal rhythm, is a viable approach to preventing VF.

Being able to control the dynamics of the heart with as few electrodes as possible is a matter of practical interest. At present we don't have reliable models of the entire organ that can be used to test control algorithms, so we have to resort to studies of different types of cardiac tissue for which such models exist. Ventricles, atria, and Purkinje fibers are examples of, respectively, three-dimensional, quasi-two-dimensional, and one-dimensional cardiac tissue. Hence, it is important to understand the limits on the tissue size that can be controlled using a single electrode, regardless of its dimensionality.

Purkinje fibers, whose physiological function is to conduct electrical excitation from the atria, through the atrioventricular node, to the ventricles, have been studied extensively as the simplest example of cardiac tissue¹⁰. Despite their relative simplicity, they share many dynam-

^{a)}Electronic mail: alejandro.garzon@correo.usa.edu.co

ical properties of the atrial and ventricular tissue, such as the transition from normal rhythm^{11,12} to alternans associated with increased pacing frequency. Different models for cardiac cells have been developed over the years (see Ref. 13 for review). The first model for Purkinje cells was developed by Noble in 1962¹⁴. Despite some limitations (no calcium cycling dynamics, incorrect conduction velocity), this model does include such important dynamical features as transition to alternans. In contrast, the updated version of this model due to DiFrancesco and Noble¹⁵, which includes more detailed calcium dynamics, fails to produce alternans. Even the most recent Purkinje models of Aslanidi *et al.*¹⁶ and Sampson *et al.*¹⁷ do not show alternans. This paper uses a model recently developed by one of us¹⁸ which correctly describes both the APD restitution dynamics and the transition to alternans.

Several methods have been used to prevent and control fibrillation^{19–25}. Echebarria and Karma²⁶ were the first to consider the feedback control of Purkinje fibers. They showed that alternans can be suppressed in the Noble model, using pacing interval adjustment (PIA) method which varies the pacing interval by an amount proportional to the difference between the action potential duration (APD) on two previous intervals. Using numerical simulations they showed that alternans can be suppressed for all pacing frequencies in fibers of length up to 0.5 cm. Furthermore, using the amplitude equation formalism they showed that PIA can only stabilize the mode with the lowest spatial frequency. This leads to the failure of control when a second unstable mode appears due to an increase in either the pacing frequency or the fiber length. These theoretical predictions were verified experimentally by Christini *et al.* in dog Purkinje fibers¹⁰.

In a previous paper²⁷ we have proposed a more general method for suppressing alternans based on model predictive control (MPC). In this approach the pacing interval is held fixed, while feedback current is applied during a brief time interval between the pacing stimuli. This approach was tested on the Noble model and numerical simulations showed that fibers of up to 1.5 cm length could be successfully controlled over the entire range of pacing frequencies. Furthermore, our analysis confirmed, without relying on the amplitude equation, that the failure of control for the PIA method is indeed due to the loss of controllability for higher-frequency modes. In the case of MPC, though, the failure was not caused by the loss of controllability, but rather by transient amplification of finite-amplitude disturbances in a linearly stable system^{28–30}.

The aim of this work is to explore the potential of continuous-time feedback control for suppressing alternans in considerably longer fibers. Continuous-time approach allows addressing the major weakness of impulsive control: transient amplification. Indeed, transient amplification is an unavoidable feature of impulsive control, which uses feedback current that is applied during a

brief time interval, once per pacing period. Disturbances can grow, uncontrolled, during the interval between one feedback impulse and the next, i.e., essentially for the entire duration of the pacing interval.

This paper is organized as follows. In Sect. II we introduce a partial differential equation (PDE) model of Purkinje fibers. Section III is devoted to the linear stability analysis of normal rhythm. The reduction of the infinite-dimensional PDE model of the fiber is discussed in Sect. IV. Impulsive and continuous-time feedback control problems are formulated in Sects. V and VI. The results are presented and discussed in Sect. VII and conclusions in Sect. VIII.

II. MODEL EQUATIONS

The electrical activity in a single cardiac cell can be described by the following system of ordinary differential equations

$$\dot{V} = \frac{1}{C_m} [\mathcal{I}_{\text{ion}}(V, \mathbf{y}) + \mathcal{I}_{\text{ext}}(t)], \quad (1a)$$

$$\dot{\mathbf{y}} = h(V, \mathbf{y}), \quad (1b)$$

where V is the transmembrane voltage, C_m is the cell membrane capacitance per unit area, \mathcal{I}_{ion} is the ionic current through the cell membrane, \mathbf{y} is a vector of variables associated with the ion channel conductance and ionic concentrations (gating variables) and \mathcal{I}_{ext} is the current applied by an external electrode which can be used for pacing and/or control. The ionic models which define the functional forms of $\mathcal{I}_{\text{ion}}(V, \mathbf{y})$ and $h(V, \mathbf{y})$ vary according to the specific type of cardiac tissue under study.

To simulate Purkinje fibers we used an ionic model with three gating variables, $\mathbf{y} = [y_1, y_2, y_3]$, recently developed by one of us¹⁸ which accurately reproduces experimental measurements, as explained below. It is convenient to use a scaled voltage variable

$$u = \frac{V - V_{\text{off}}}{V_{\text{sc}}}, \quad (2)$$

where V_{off} and V_{sc} are chosen so that u takes values mostly in the interval $[0, 1]$. We used the following parameters: $C_m = 12 \mu\text{F}/\text{cm}^2$, $V_{\text{sc}} = 100 \text{ mV}$, $V_{\text{off}} = -84 \text{ mV}$ following Ref. 14

Equations (1a) and (1b) can be gathered into a single equation

$$\dot{\mathbf{z}} = F(\mathbf{z}) + j_{\text{ext}}(t)\hat{\mathbf{u}}, \quad (3)$$

where the state variable now is the column vector $\mathbf{z} = [u, \mathbf{y}]$, $j_{\text{ext}} = \mathcal{I}_{\text{ext}}/(C_m V_{\text{sc}})$ and $\hat{\mathbf{u}} = [1, 0, 0, 0]$. To describe the electrical activity on a fiber of length L , we introduce an independent variable x indicating the position along the fiber and generalize (3) to a PDE

$$\partial_t \mathbf{z} = D \partial_x^2 \mathbf{z} + F(\mathbf{z}) + j_{\text{ext}}(x, t)\hat{\mathbf{u}}, \quad (4)$$

where $D = D_{11}\hat{\mathbf{u}}\hat{\mathbf{u}}^\dagger$ and the diffusion constant D_{11} describes electric conductivity between neighboring cells. Vanishing-electric-current boundary conditions are imposed at both ends: $\partial_x u|_{x=0,L} = 0$.

The external current density $j_{\text{ext}}(x, t) = j_p(x, t) + j_c(x, t)$ accounts for both pacing and feedback control. Pacing is applied by an electrode located at $x = x_p$ near the left end ($x = 0$) of the fiber,

$$j_p(x, t) = I_p(t)g(x - x_p), \quad (5)$$

where $g(x)$ is a narrow spatial profile which represents tissue polarization. The pacing current $I_p(t)$ consists of a periodic train of pulses of duration $\Delta T = 5$ ms

$$I_p(t) = Q_p \sum_{n=0}^{\infty} H_{\Delta T}(t - t_n), \quad (6)$$

where $t_n = nT$ with T the pacing period, Q_p is the total charge of each pacing stimulus, and we have defined

$$H_\tau(t) = \begin{cases} \tau^{-1}, & 0 \leq t \leq \tau \\ 0, & \text{otherwise.} \end{cases} \quad (7)$$

The feedback current $I_c(t)$ corresponds to one strand of cardiac cells. Purkinje fibers contain a bundle of multiple strands. Each strand consists of cells that are about $30 \mu\text{m} \times 10 \mu\text{m} \times 200 \mu\text{m}$ in size³¹, so that the perimeter is $P_c \approx 80 \mu\text{m}$ and the cross sectional area is $A_c \approx 300 \mu\text{m}^2$. The bundle has a radius that ranges from $66 \mu\text{m}$ to $147 \mu\text{m}$ ^{32,33} and hence contains about 100 strands. Assuming the current injected by an electrode quickly diffuses across all strands, the corresponding control current applied to the entire fiber should be approximately a hundred times larger than the values computed for a single strand below.

Each pacing pulse produces an excitation wave that travels down the fiber. The dynamics of cardiac tissue is conveniently described in terms of the APD, defined, for a particular location x , as the time interval during which the voltage surpasses some threshold value, u_{th} . The APD is therefore a function of x and the pacing interval n , denoted as $\text{APD}_n(x)$. Depending on the pacing period T , Purkinje fibers present two asymptotic regimes: when T is larger than some critical value T_c , the APD is constant from beat to beat, $\text{APD}_n(x) = \text{APD}_{n+1}(x)$ for all x . This regime corresponds to normal rhythm; when $T < T_c$ the APD alternates between a longer and a shorter value from beat to beat. This regime corresponds to the state of alternans. Alternans could be *concordant*, if the difference $\text{APD}_{n+1}(x) - \text{APD}_n(x)$ has the same sign along the entire fiber or *discordant* if it does not. Hence, discordant alternans presents one or more locations (nodes) $x_{k,n}$, $k = 1, 2, \dots$, for which $\text{APD}_{n+1}(x_{k,n}) - \text{APD}_n(x_{k,n}) = 0$. Furthermore, the nodes can move along the fiber or slow down and stop, producing either traveling or standing discordant alternans.

Unlike previous models of Purkinje fibers, the ionic model¹⁸ accurately reproduces the experimentally measured bifurcation diagram of asymptotic APD as a function of T , the shape of the action potential, and the action potential restitution curve. Furthermore, the model exhibits traveling discordant alternans in agreement with experimental observations. The diffusion constant is the only parameter with the units of length and hence determines the length scale for the spatial variations of the solution. We set $D_{11} = 10^{-4} \text{ cm}^2/\text{ms}$, so that, for parameters of the ionic model taken from Ref. 18, a 2 cm-long fiber would fit traveling discordant alternans with one node as observed in experiments^{10,34}. We further assume that the fiber is paced at the left end, $x_p = 0$ and choose

$$g(x) = \frac{H_a(x)}{P_c C_m V_{sc}}, \quad (8)$$

where the ‘‘width’’ of the electrode $a = 0.07$ cm is very small compared to the fiber length L .

Feedback is applied by an electrode located at $x = x_c$,

$$j_c(x, t) = I_c(t)g(x - x_c), \quad (9)$$

which may or may not be collocated with the pacing electrode. Our goal is to determine the location x_c of the control electrode and a control current, $I_c(t)$ which can suppress the state of alternans in favor of normal rhythm, when the latter becomes unstable, for fiber lengths comparable to their physiological dimension (up to about 4 cm). The solution to this problem is presented below.

III. LINEAR STABILITY ANALYSIS

When T is decreased below T_c , the time-periodic solution describing normal rhythm does not disappear, but becomes unstable and is replaced by the (stable) state of alternans. To determine the stability of normal rhythm, we apply Floquet analysis following an approach similar to that used in Ref. 27. The time- T periodic orbit $\mathbf{z}_0(x, t)$ is found by solving the equation

$$\mathbf{z}_0(x, 0) = G[\mathbf{z}_0(x, 0); T, 0], \quad (10)$$

where $G[\cdot; T, 0]$ is the time evolution operator which advances the solution of (4) from $t = 0$ to $t = T$. Eq. (10) is solved using the Newton-Krylov method^{27,35}. To avoid the non-differentiability of the evolution operator, the Heaviside step functions $\Theta(x)$ used in the original formulation of the ionic model¹⁸ were replaced by their smoothed versions

$$\Theta_\nu(x) = \frac{1}{2} \left[1 + \tanh\left(\frac{x}{\nu}\right) \right] \quad (11)$$

with $\nu = 10^{-3}$. The operator G is implemented numerically by advancing in time the solution of (4) using the fourth order Runge-Kutta method with a time step of

2.5×10^{-3} ms. A second order central finite difference approximation is used for the diffusion term with a mesh size $\Delta x = 0.01$ cm.

To determine the stability of $\mathbf{z}_0(x, t)$, we consider the evolution of the deviation $\delta\mathbf{z} = \mathbf{z}(x, t) - \mathbf{z}_0(x, t)$, given in the linear approximation by

$$\partial_t \delta\mathbf{z} = J_{\mathcal{N}}(t)\delta\mathbf{z} - j_c \hat{\mathbf{u}}, \quad (12)$$

where $J_{\mathcal{N}}(t) = \partial_x^2 + J_F(t)$ and $J_F(t) = DF/D\mathbf{z}|_{\mathbf{z}_0(x, t)}$ is a time-periodic Jacobian operator. Let $U(t, 0)$ denote the time evolution operator that advances the solution of (12) in time, in the absence of feedback ($j_c = 0$),

$$\delta\mathbf{z}(x, t) = U(t, 0)\delta\mathbf{z}(x, 0). \quad (13)$$

The stability of normal rhythm is determined by the eigenvalues λ_i of the operator $U(T, 0)$ (Floquet multipliers). The eigenvalues and the corresponding right eigenfunctions $\mathbf{e}_i(x, 0)$ satisfy

$$U(T, 0)\mathbf{e}_i(x, 0) = \lambda_i \mathbf{e}_i(x, 0) \quad (14)$$

and are calculated numerically using the Arnoldi method³⁶ implemented by the MATLAB (Mathworks, Inc.) function `eigs`. Normal rhythm is unstable when at least the leading eigenvalue lies outside the unit circle, $|\lambda_1| > 1$ (where the eigenvalues are sorted in order of decreasing absolute value, $|\lambda_1| \geq |\lambda_2| \geq |\lambda_3| \geq \dots$).

The number of unstable eigenvalues for different fiber lengths L and pacing periods T is summarized in Fig. 1. Normal rhythm becomes unstable (and small perturbations evolve toward the state of alternans) at a critical value $T_c \approx 205$ ms for the range of lengths shown. A region of stability is also found for some lengths for $152 \text{ ms} < T < 162 \text{ ms}$. However, we found that in this region normal rhythm is not the only attractor, as some initial conditions evolve toward a state of sustained alternans of large amplitude. For example, for $L = 2$ cm and $T = 158$ ms, the APD alternates between, roughly, 90 ms and 140 ms.

For canine Purkinje fibers, the alternans branches of the experimentally measured bifurcation diagram of APD as a function of period meet at a sharp angle suggesting a border-collision bifurcation. Onset of alternans through border-collision bifurcations has been observed in other types of cardiac tissue (See Ref. 37 and references therein). Border-collision bifurcations occur when the surface in the parameter space is crossed at which the Jacobian experiences a discontinuity. The crossing of this surface manifests as a sudden jump of the eigenvalues. The ionic model was tuned to reproduce the APD bifurcation diagram typical of a border-collision bifurcation. Since the discontinuities of the original ionic model were replaced in this work with smooth, although rapidly varying, functions, the leading eigenvalues (shown in Fig. 2) do not change discontinuously, but rather vary quickly with T close to the onset of the instability.

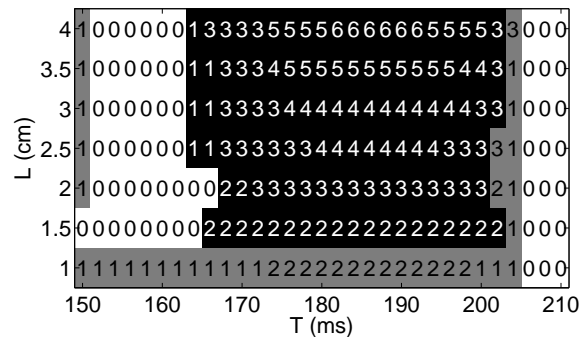


FIG. 1. Stability diagram showing the number of unstable eigenvalues for normal rhythm. White indicates the region in parameter space where normal rhythm is stable. Impulsive control successfully suppresses alternans in the gray region. Continuous-time control is successful in the gray and black regions.

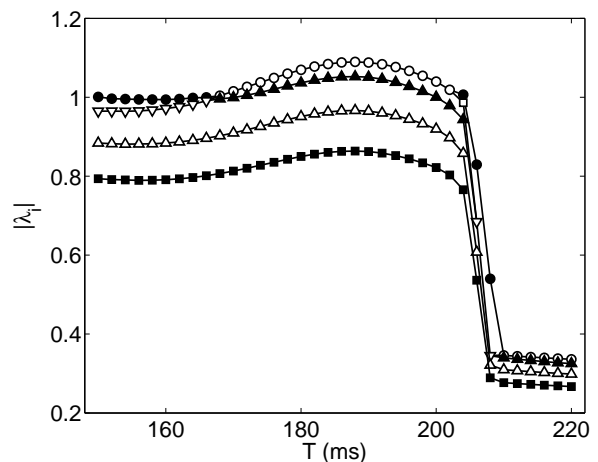


FIG. 2. Absolute value of the leading eigenvalues for $L = 2$ cm. Real eigenvalues: $|\lambda_1|$ (filled circles), $|\lambda_2|$ (open squares), $|\lambda_3|$ (upward filled triangles), $|\lambda_4|$ (upward open triangles), $|\lambda_5|$ (filled squares); Complex conjugate eigenvalues: $|\lambda_1| = |\lambda_2|$ (open circles), $|\lambda_2| = |\lambda_3|$ (downward open triangles)

IV. GALERKIN PROJECTION

In order to make the control problem tractable, a finite-dimensional representation of the dynamics is obtained by means of a Galerkin projection of the perturbation $\delta\mathbf{z}$ onto a basis $\tilde{\mathbf{e}}_i(x, t)$, $i = 1, 2, \dots, m$, defined below,

$$\delta\mathbf{z}(x, t) = \sum_{i=1}^m \xi_i(t) \tilde{\mathbf{e}}_i(x, t). \quad (15)$$

This allows reduction of the infinite-dimensional dynamics described by the PDE (4) to the dynamics of the coefficients $\xi_i(t)$, referred to henceforth as the *modal amplitudes*. Retaining only the dominant modes with $|\lambda_i| > 0.1$ in (15) ensures a representation sufficiently accurate for the control problem (this corresponds to m ranging from 7 for $L = 1$ cm to 25 for $L = 4$ cm).

Let us define the left eigenfunctions $\mathbf{f}_i(x, 0)$ which satisfy

$$U^\dagger(T, 0)\mathbf{f}_i(x, 0) = \lambda_i^* \mathbf{f}_i(x, 0). \quad (16)$$

With the proper normalization, the left and right eigenfunctions satisfy the orthogonality condition

$$\langle \mathbf{f}_i(x, 0), \mathbf{e}_k(x, 0) \rangle = \delta_{ik}. \quad (17)$$

Next we extend the definition of basis functions $\mathbf{e}_i(x, 0)$ and $\mathbf{f}_i(x, 0)$ to times other than $t = 0$. Let's define

$$\mathbf{e}_i(x, t) \equiv U(t, 0)\mathbf{e}_i(x, 0) \quad (18)$$

and

$$\mathbf{f}_i(x, t) \equiv (\lambda_i^*)^{-1} U^\dagger(T, t)\mathbf{f}_i(x, 0) \quad (19)$$

In using the definition (19) for $t > T$ recall that $U(t_f, t_i) = U^{-1}(t_i, t_f)$. (Incidentally we note that, as shown in Ref. 27, $\mathbf{e}_i(x, t)$ and $\mathbf{f}_i(x, t)$ are respectively the eigenfunctions of $U(\tau+T, \tau)$ and $U^\dagger(\tau+T, \tau)$, where $\tau = t \bmod T$). Definitions (18) and (19) apply for all $t > 0$. In particular, for $t = \tau + nT$, $0 \leq \tau < T$, $n = 1, 2, \dots$, they imply that

$$\mathbf{e}_i(x, \tau + nT) = \lambda_i^n \mathbf{e}_i(x, \tau), \quad (20)$$

and

$$\mathbf{f}_i(x, \tau + nT) = (\lambda_i^*)^{-n} \mathbf{f}_i(x, \tau). \quad (21)$$

While the eigenfunctions of the evolution operator, thus defined, dramatically simplify the description of the linearized dynamics by decoupling the mode amplitudes, they are not time-periodic. It is more convenient to use a basis which is both time-periodic and time-continuous. Such a basis can be constructed by multiplying $\mathbf{e}_i(x, t)$ by an exponential factor:

$$\tilde{\mathbf{e}}_i(x, t) = e^{-\omega_i t} \mathbf{e}_i(x, t) \quad (22)$$

where ω_i is the Floquet exponent

$$\omega_i = \frac{\ln \lambda_i}{T}. \quad (23)$$

The corresponding adjoint basis is defined by

$$\tilde{\mathbf{f}}_i(x, t) = e^{\omega_i^* t} \mathbf{f}_i(x, 0) \quad (24)$$

Using (17) it is easy to verify that $\tilde{\mathbf{e}}_i(x, t)$ and $\tilde{\mathbf{f}}_i(x, t)$ satisfy the orthogonality condition

$$\langle \tilde{\mathbf{f}}_i(x, t), \tilde{\mathbf{e}}_k(x, t) \rangle = \delta_{ik}. \quad (25)$$

Next we derive the evolution equation for the modal amplitudes $\xi_i(t)$. Substituting (15) into (12) and rearranging terms we obtain

$$\begin{aligned} \sum_{i=1}^m \dot{\xi}_i \tilde{\mathbf{e}}_i &= \sum_{i=1}^m \omega_i \xi_i \tilde{\mathbf{e}}_i + \\ &+ \sum_{i=1}^m \xi_i e^{-\omega_i t} [J_{\mathcal{N}} \mathbf{e}_i - \partial_t \mathbf{e}_i] + j_c \hat{\mathbf{u}}. \end{aligned} \quad (26)$$

Equation (18) implies

$$\partial_t \mathbf{e}_i = J_{\mathcal{N}} \mathbf{e}_i, \quad (27)$$

therefore the expression in square brackets in (26) vanishes. Applying the operation $\langle \tilde{\mathbf{f}}_i(x, t), \cdot \rangle$ to the remaining terms of (26) and using the orthogonality condition (25) we obtain

$$\dot{\xi}_i = \omega_i \xi_i + \langle \tilde{\mathbf{f}}_i(x, t), j_c(x, t) \hat{\mathbf{u}} \rangle \quad (28)$$

Substitution of (9) into (28) yields

$$\dot{\xi}_i = \omega_i \xi_i + \tilde{b}_i(t) I_c(t) \quad (29)$$

where

$$\tilde{b}_i(t) = \langle \tilde{\mathbf{f}}_i(x, t), g(x - x_c) \hat{\mathbf{u}} \rangle \quad (30)$$

is a periodic function, which incorporates the dependence on the location of the control electrode.

For the purposes of impulsive control²⁷ the dynamical description can be simplified further by reducing the system of ODEs (29) to a stroboscopic section $\xi_i^n = \xi_i(t_n)$ of the flow, yielding a map:

$$\xi_i^{n+1} = \lambda_i \xi_i^n + \lambda_i \int_0^T b_i(s) I_c^n(s) ds \quad (31)$$

where $b_i(s) = \langle \mathbf{f}_i(x, s), g(x - x_c) \hat{\mathbf{u}} \rangle$ and $I_c^n(s) = I_c(s + nT)$, $0 \leq s < T$. In order to reduce transient amplification associated with the growth of unstable modes between the instances at which impulsive feedback is applied, feedback needs to be adjusted at a higher rate than once per pacing interval (e.g., N times per pacing interval). In the limit $N \rightarrow \infty$ one obtains continuous-time feedback. We describe and compare these different approaches below.

V. IMPULSIVE FEEDBACK

Impulsive feedback relies on a sequence of brief square pulses of control current

$$I_c^n(t) = I^n H_{\Delta t}(t - \tau) \quad (32)$$

applied, one pulse per period, at times $t'_n = nT + \tau$, where $0 \leq \tau < T$, with pulse duration equal to one time step Δt . Since Δt is much shorter than any dynamical time scale, the physical effect of each pulse is determined by the net (dimensionless) charge $q_n = I^n \Delta t$ injected. Substituting (32) into (31), we arrive at the linear time-invariant map

$$\boldsymbol{\xi}^{n+1} = A \boldsymbol{\xi}^n + B q_n, \quad (33)$$

where $\boldsymbol{\xi}^n = [\xi_1^n, \xi_2^n, \dots, \xi_m^n]$, A is an $m \times m$ diagonal matrix with elements $A_{ii} = \lambda_i$ and B is a vector with elements $B_i = \lambda_i b_i(\tau)$.

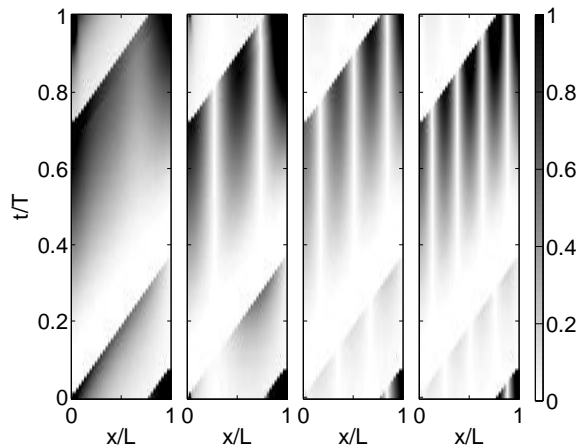


FIG. 3. Adjoint eigenfunctions $|f_i^u(x, t)|$ for $L = 2$ cm and $T = 180$ ms. From left to right, $i = 1, 3, 4, 5$. Modes 1 and 2 are complex conjugate.

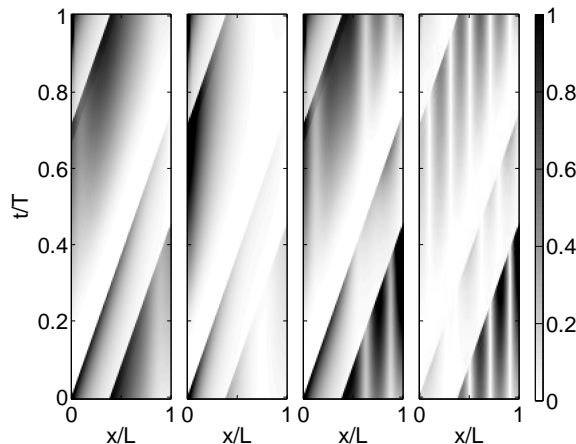


FIG. 4. Adjoint eigenfunctions $|f_i^u(x, t)|$ for $L = 4$ cm and $T = 180$ ms. From left to right, $i = 1, 3, 4, 6$. Modes 1 and 2 are complex conjugate, as well as modes 4 and 5.

Given that $g(x)$ has a narrow profile, $B_i(\tau) \approx f_i^u(x_c, \tau)$, where f_i^u is the voltage component of \mathbf{f}_i , and

$$\xi_i^{n+1} \approx \lambda_i \xi_i^n + f_i^u(x_c, \tau) q_n, \quad (34)$$

Therefore, as discussed in Ref. 27, the value of $f_i^u(x_c, \tau)$ describes the effect of the stimulus q_n on the dynamics of mode i . In particular, when $f_i^u(x_c, \tau) = 0$ for some unstable eigenvalue, the corresponding mode becomes uncontrollable. On the other hand, larger values of $|f_i^u(x_c, \tau)|$ allow the use of smaller control stimuli. Hence it is convenient to choose the position of the control electrode x_c and the timing of the control stimulus which maximize $|f_i^u(x, t)|$.

Figs. 3 and 4 show the magnitude of the adjoint eigenfunctions for the leading modes of 2 cm- and 4-cm long fibers paced with the period of 180 ms. All adjoint eigenfunctions have pronounced local maxima at the left end ($x = 0$) of the fiber, for all L and T . Furthermore, the

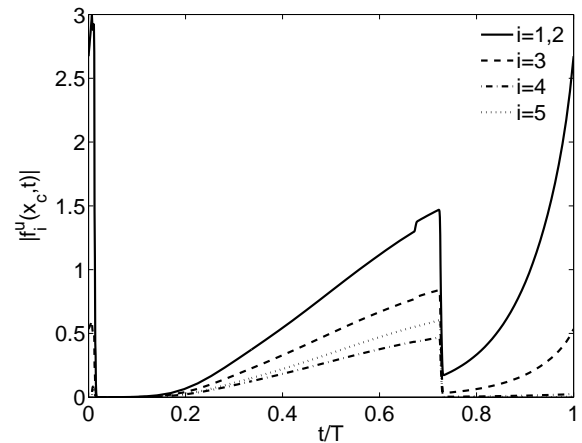


FIG. 5. The magnitude of the the adjoint eigenfunctions for $x_c = 0$, $L = 2$ cm, and $T = 180$ ms.

temporal positions t_0 of the corresponding local maxima for different modes coincide (cf. Fig. 5) for all T and L . This is a robust feature which is due to the local dynamics of the gating variables. In the unstable range $150 \text{ ms} < T < 204 \text{ ms}$, t_0/T is independent of L and is weakly dependent on T , as Fig. 6 shows.

The global maxima of $|f_i^u(x, t)|$, for all modes, are reached along the straight line

$$t_x = \text{mod}(t_0 + x/c_v, T), \quad (35)$$

where c_v is the conduction velocity. However, the value of $f_i^u(x, t_x)$ oscillates with different wavelength for different modes, vanishing for some values of x and reaching a maximal value for others. In particular, the nodes of $f_i^u(x, t_x)$ correspond to the choices of x_c and τ , which render mode i uncontrollable and should be avoided. Moreover, the maxima for different modes do not coincide, so there is no unique best choice of x_c . The only choice that guarantees controllability of all modes for any L and T is $x_c = 0$ and $\tau \approx t_0$. This is consistent with the results of the original study²⁷ which found that, for the Noble model, the choice $x_c = x_p$ guaranteed controllability, motivating the use of the pacing electrode also to apply the feedback. We make the same choice here, setting $x_c = x_p = 0$ and $\tau = t_0 - \Delta t$.

The control objective can be achieved by using the feedback law

$$I^n \Delta t = q_n = K \xi^n, \quad (36)$$

where $\xi_i^n = \xi_i(t_n)$ and

$$\xi_i(t) = \langle \tilde{\mathbf{f}}_i(x, t), \delta \mathbf{z}(x, t) \rangle. \quad (37)$$

The gain matrix K is calculated using the linear quadratic regulator (LQR) method³⁸, which aims to minimize the quadratic form

$$V_1 = \sum_{n=1}^{\infty} \left[(\xi^n)^\dagger Q \xi^n + R q_n^2 \right] \quad (38)$$

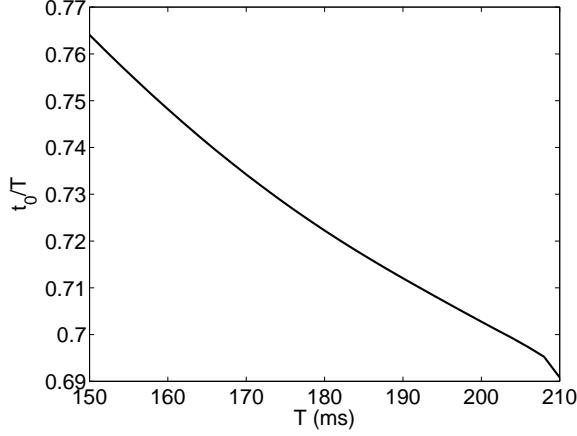


FIG. 6. Temporal position t_0 of the medial local maxima of $|f_i^u(x_c, t)|$ (see Fig. 5) for $x_c = 0$ and $L = 2$ cm.

where Q is a positive-definite matrix and R is a positive constant. Our objective is to minimize the deviation $\delta\mathbf{z}$ from the time-periodic solution describing normal rhythm. Restricted to the Galerkin projection onto the m leading modes and the values at the stroboscopic sections $t = t_n$, it is equal to minimizing the projection

$$P_m \delta\mathbf{z}(x, t) = \sum_{i=1}^m \xi_i(t) \tilde{\mathbf{e}}_i(x, t). \quad (39)$$

which is achieved by setting $Q_{ik} = \langle \mathbf{e}_i(x, 0), \mathbf{e}_k(x, 0) \rangle$, so that

$$(\boldsymbol{\xi}^n)^\dagger Q \boldsymbol{\xi}^n = \|P_m \delta\mathbf{z}(x, t_n)\|_2^2. \quad (40)$$

We computed the feedback gain using the MATLAB function `dpre` (available through the *MATLAB exchange* website³⁹), which solves the discrete Riccati equation obtained by minimizing (38).

VI. PIECEWISE CONSTANT FEEDBACK

Instead of using impulsive control, one could apply the feedback at all times. In practice the feedback cannot be varied continuously, so we will treat the control current as constant on sub-intervals of duration $\delta T = T/N$,

$$I_c^n(t) = I^{nk}, \quad (k-1)\delta T \leq t < k\delta T, \quad (41)$$

where $k = 1, 2, \dots, N$. Substituting (41) into (31) we arrive at the discrete map

$$\boldsymbol{\xi}^{n+1} = A \boldsymbol{\xi}^n + B I^n \quad (42)$$

where B is an $m \times N$ matrix with elements

$$B_{ik} = \lambda_i \int_{(k-1)\delta T}^{k\delta T} b_i(s) ds \quad (43)$$

and $I^n = [I^{n1}, I^{n2}, \dots, I^{nN}]$. The control current is again given by the feedback law

$$I^n = K \boldsymbol{\xi}^n, \quad (44)$$

where K is an $N \times m$ matrix obtained by minimizing the quadratic form

$$V_2 = \sum_{n=0}^{\infty} \left[(\boldsymbol{\xi}^n)^\dagger Q \boldsymbol{\xi}^n + \frac{R}{N} \|I^n\|_2^2 \right]. \quad (45)$$

While this method allows greater flexibility in optimizing the control current, it has a limitation. The feedback is computed based on the information about the system state collected only at stroboscopic sections $t = t_n$ (i.e., once per pacing interval).

We can improve the feedback algorithm further by computing the control current as a function of the latest available system state, i.e., the state at the beginning of each sub-interval

$$t_{n,k} = t_n + (k-1)\delta T. \quad (46)$$

To describe the discrete-time dynamics it is convenient to relabel the times $t_{n,k}$ using a single index as

$$r_l \equiv l\delta T = t_{n,k}, \quad l = 0, 1, 2, \dots \quad (47)$$

Whenever an equation contains mixed single and double indexing it must be understood that the following relations between the indices [which are consequences of (47) and (46)] hold

$$n = \lfloor l/N \rfloor, \quad (48)$$

$$k = (l \bmod N) + 1, \quad (49)$$

with $\lfloor x \rfloor$ denoting the integer part of x . Similarly, we label with a single index the control current on a sub-interval as

$$I_l = I^{nk}. \quad (50)$$

The flow of (29) from r_l to r_{l+1} is given by

$$\boldsymbol{\xi}_i^{l+1} = e^{\omega_i \delta T} \boldsymbol{\xi}_i^l + I_l e^{\omega_i k \delta T} \int_{(k-1)\delta T}^{k\delta T} b_i(s) ds. \quad (51)$$

where $\boldsymbol{\xi}_i^l = \xi_i(r_l)$. Gathering the maps (51) for the m leading modes we obtain

$$\boldsymbol{\xi}^{l+1} = A' \boldsymbol{\xi}^l + B^l I_l, \quad (52)$$

where $\boldsymbol{\xi}^l = [\xi_1^l, \xi_2^l, \dots]$, A' is an $m \times m$ diagonal matrix with elements $A'_{ii} = e^{\omega_i \delta T} = A_{ii}^{1/N}$ and B^l is a vector with elements

$$B_i^l = e^{\omega_i k \delta T} \int_{(k-1)\delta T}^{k\delta T} b_i(s) ds. \quad (53)$$

The vector B^l is time-periodic: $B^{l+N} = B^l$. The control current is again given by the feedback law

$$I_l = K_l \xi^l, \quad (54)$$

where the vector ξ^l is defined by (37) evaluated at $t = r_l$. The gain K_l is also time-periodic: $K_{l+N} = K_l$ and is computed by minimizing the quadratic form

$$V_3 = \sum_{l=1}^{\infty} \left[(\xi^l)^\dagger Q^l \xi^l + \frac{R}{N} I_l^2 \right], \quad (55)$$

where Q^l is an $m \times m$ time-periodic matrix with elements $Q_{ik}^l = \langle \tilde{\mathbf{e}}_i(x, r_l), \tilde{\mathbf{e}}_k(x, r_l) \rangle$. Minimization of (55) leads to a discrete time-periodic Riccati equation, which was solved using the cyclic QZ factorization approach of Hench and Laub⁴⁰ implemented by the function **dpred**.

We will refer to the feedback (44) and (54), respectively, as asynchronous and synchronous continuous-time control. This notation reflects the fact that in the latter case the control current is computed based on the system state at the current time, while in the former case a time-delayed system state is used.

It should be pointed out that the elements of matrices A , A' , B , and B^l are in general complex, and so are the modal amplitudes ξ_i^n . These complex elements do, however, come in complex conjugate pairs, so that the functions V_1 , V_2 , and V_3 are real and so should be the solutions for the control current. We found that the gain matrices calculated by **dpred** indeed produced a real control current (up to a negligible imaginary part, arising due to finite precision of numerical calculations, which was discarded). The matrices can be made real by an appropriate coordinate transformation. The control currents obtained using **dpred** in the new coordinates, however, were the same as those calculated for the original complex maps. For the time invariant maps we also used the function **dlqr** from MATLAB's control system toolbox, which does not accept complex matrices as input arguments. Again, the control currents were identical to those obtained with **dpred** to within the precision of numerical calculations.

VII. RESULTS

Impulsive control (IC), asynchronous continuous-time control (ACT), and synchronous continuous-time control (SCT) were tested by using, respectively, the control currents (32), (41), and (50) in the original PDE model (4). To simulate a gradual reduction of the pacing interval, for each T , we evolved initial conditions corresponding to the solution for normal rhythm with period $T + 2$ ms and checked whether feedback was successful in suppressing the instability caused by the 2 ms reduction in the pacing interval.

The regions in the (L, T) parameter space where different control methods succeed (or fail) are shown in Fig. 1.

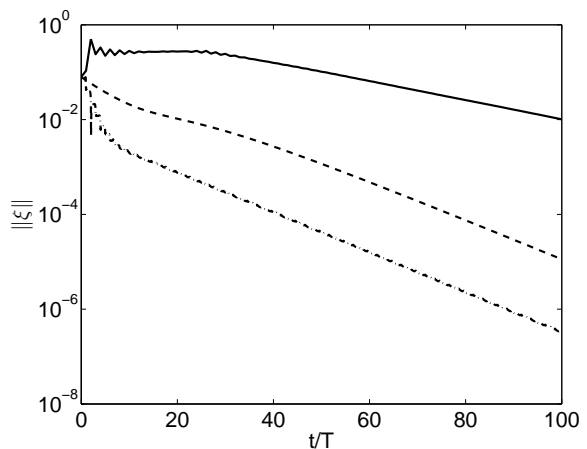


FIG. 7. Disturbance magnitude $\|\xi(t)\|$ for IC (solid line), ACT (dashed line), and SCT (dot-dashed line). $L = 1$ cm, $T = 188$ ms, $R = 10^5$, and $N = 20$.

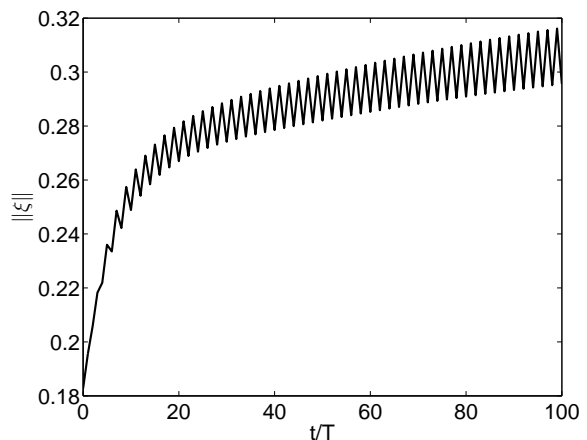


FIG. 8. Disturbance magnitude $\|\xi(t)\|$ for impulsive control; $L = 1.5$ cm and $T = 202$ ms.

We find that continuous-time control (both synchronous and asynchronous) succeeds in the entire investigated range of L and T where normal rhythm is unstable, which includes fibers up to 4 cm long. Impulsive control, on the other hand, is only effective for fibers with length of 1 cm and below. Just as in the case of the Noble model²⁷, here IC fails due to transient amplification of initial disturbances.

Figure 7 shows the norm of the deviation $\|\xi(t)\|$ from normal rhythm for a 1 cm-long fiber. For such a short fiber IC, ACT, and SCT all succeed. Of the three control methods, IC is the only one that exhibits transient amplification. As Fig. 8 illustrates, for longer fibers transient amplification drives the dynamics into the nonlinear regime where (12) is no longer a valid approximation, leading to the failure of impulsive control.

For even longer fibers ($L = 4$ cm) transient amplification manifests itself even for ACT, as Fig. 9 illustrates, with $\|\xi(t)\|$ slightly exceeding $\|\xi(0)\|$ for a brief

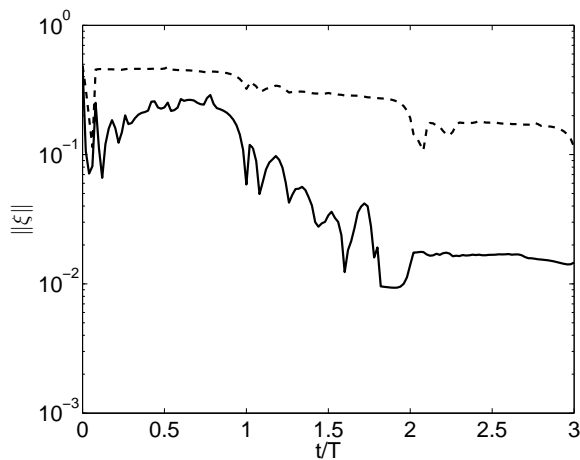


FIG. 9. Disturbance magnitude $\|\xi(t)\|$ for ACT (dashed line) and SCT (solid line). $L = 4$ cm, $T = 168$ ms, $R = 10^5$ and $N = 50$.

interval of time. SCT is again found to be superior to ACT for long fibers: it suppresses the disturbance faster and without transient amplification. However, even for ACT, the amount of amplification is nowhere near large enough to bootstrap the nonlinear instability, which explains why continuous-time control is successful where impulsive control fails.

Even for short fibers where IC succeeds, ACT still remains superior, decreasing the disturbance $\|\xi(t)\|$ at a much higher rate (cf. Fig. 7). SCT suppresses the initial disturbance even faster than ACT, illustrating the clear advantage of using the most up-to-date information about the state of the system.

Figure 10 shows the effect of increasing the number of sub-intervals on ACT control. We find that while the increase in the temporal resolution has a large impact on the initial decay rate, the asymptotic decay rate is found to be independent of N . This is understandable: the asymptotic decay rate is controlled by the slowest (least stable) mode of the closed-loop system. While the fine structure (high-frequency components) of the control current resolved at large N strongly affect the dynamics of fast (strongly stable) modes, it has virtually no effect on the dynamics of slow (weakly stable) modes.

The decrease in $\|\xi(t)\|$ with N is also easy to understand. The control current $I_c^n(t)$ on a given pacing interval is a function from within a vector space \mathcal{S}^N of dimension N . Furthermore, \mathcal{S}^N is a subset of \mathcal{S}^{kN} for any integer $k > 1$. In the particular example shown in Fig. 10, $N = 4$ and $k = 5$ (or $N = 20$ and $k = 5$). The minimal value of V_2 over \mathcal{S}^{kN} is less than or equal to the minimum over \mathcal{S}^N , leading to a more optimal control (and lower values of $\|\xi(t)\|$). For $N = 20$ the feedback is only slightly sub-optimal, since increasing the number of intervals to $N = 100$ changes $\|\xi(t)\|$ very little. This is further confirmed by Fig. 11, which compares the control current $I_c(t)$ for different numbers of subintervals. As

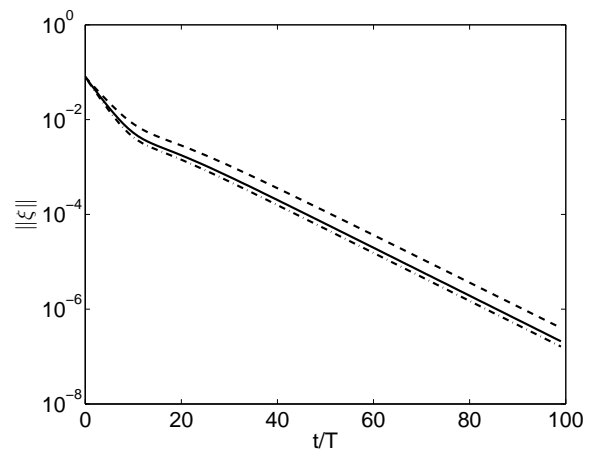


FIG. 10. Disturbance magnitude $\|\xi(t)\|$ for ACT. Number of sub-intervals: $N = 4$ (dashed line), $N = 20$ (solid line), $N = 100$ (dot-dashed line); $L = 1$ cm, $T = 188$ ms, $R = 10^4$.

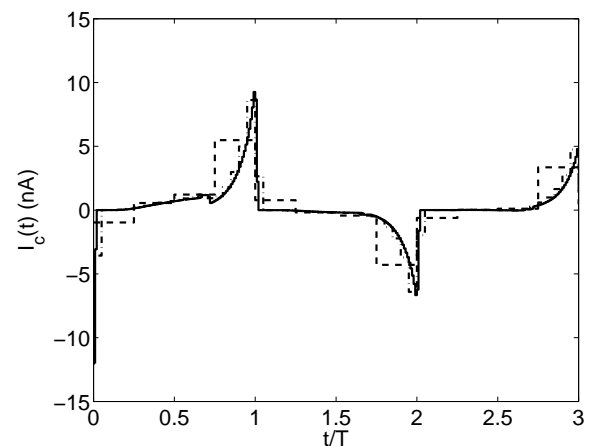


FIG. 11. Control current $I_c(t)$ for ACT. Number of sub-intervals: $N = 4$ (dashed line), $N = 20$ (dot-dashed line), $N = 100$ (solid line); $L = 1$ cm, $T = 188$ ms, $R = 10^4$.

N increases, the piecewise constant control current approaches a limit which corresponds to the optimal time-continuous feedback. At $N = 100$ the piecewise constant approximation is virtually indistinguishable from the smooth limiting shape.

The effect of increasing the number of sub-intervals is largely the same for SCT. Figure 12 shows the evolution of the disturbance magnitude $\|\xi\|$ for $N = 4, 20$ and 100 . As expected, feedback computed for higher N suppresses disturbances more rapidly. The difference is especially noticeable at early times when a large number of modes, both slow and fast, are excited. The feedback is computed using a truncation which ignores the fast (strongly stable) modes. The initial disturbance is a superposition of both slow and fast modes and while ACT recomputes the modal amplitudes once per period, SCT recomputes the modal amplitudes much more frequently, leading to a substantially more accurate estimate of the system state

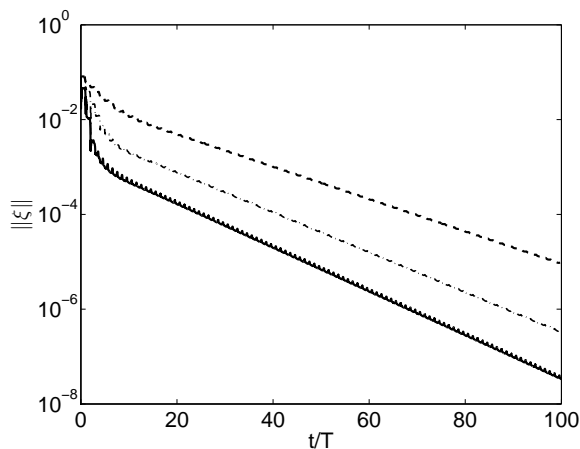


FIG. 12. Disturbance magnitude $\|\xi(t)\|$ for SCT. Number of sub-intervals: $N = 4$ (dashed line), $N = 20$ (dot-dashed line), $N = 100$ (solid line); $L = 1$ cm, $T = 188$ ms, $R = 10^5$.

and, hence, substantially more efficient feedback.

At longer times, when the fast modes have already been suppressed, the disturbance primarily contains the slow (weakly stable) modes and the advantage of SCT over ACT in terms of accurately resolving the system state disappears. Hence the asymptotic rate at which the disturbance decays is the same for ACT and SCT, as Fig. 7 illustrates. The rate also becomes essentially independent of N , as Fig. 12 shows, with the N -dependence of $\|\xi\|$ due primarily to the differences in the closed-loop dynamics at early times.

Figure 13 shows how the control current for SCT depends on the number of sub-intervals. Similarly to ACT (cf. Fig. 11), $I_c(t)$ approaches a limiting shape as N increases. For both SCT and ACT, this limiting shape is smooth, with the exception of a couple of jumps per period. A quick comparison with Fig. 14 shows that the locations of these jumps correspond to the time instances when the adjoint eigenfunctions $f_i^u(x_c, t)$ of the leading modes change discontinuously. Similarly, the maxima of $|I_c(t)|$ correspond to the maxima of $|f_i^u(x_c, t)|$. This result is quite intuitive: the magnitude of $f_i^u(x_c, t)$ determines how strongly the control current affects the dynamics of the leading (unstable) modes. Hence, optimal feedback is the strongest (weakest) where $|f_i^u(x_c, t)|$ is the largest (smallest).

VIII. CONCLUSIONS

Destabilization of normal rhythm was investigated in a quantitatively accurate model of Purkinje fibers. It was shown that the instability can be suppressed, in the entire range of pacing frequencies where it arises, by application of feedback control applied through the pacing electrode. The feedback current computed using three different methods was compared. We found that impul-

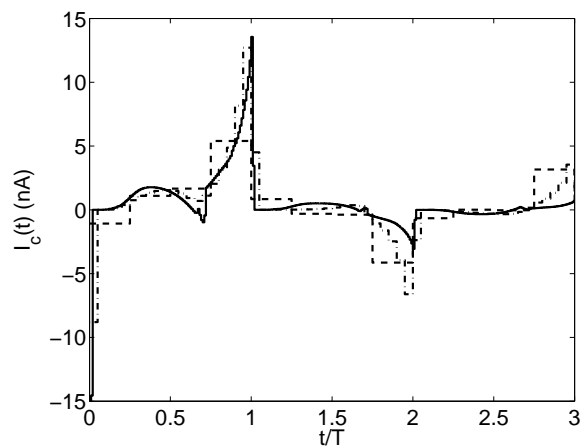


FIG. 13. Control current $I_c(t)$ for SCT. Number of sub-intervals: $N = 4$ (dashed line), $N = 20$ (dot-dashed line), $N = 100$ (solid line); $L = 1$ cm, $T = 188$ ms, $R = 10^5$.

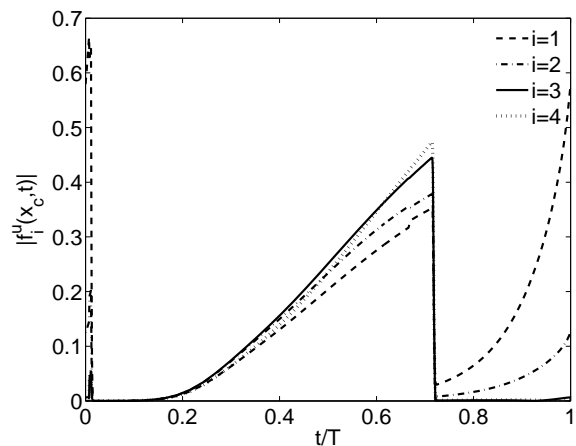


FIG. 14. The magnitude of the the adjoint eigenfunctions for $x_c = 0$, $L = 1$ cm, and $T = 188$ ms.

sive control which uses electric current applied during a brief interval between pacing stimuli is successful only for short fibers (about 1 cm long). Transient amplification of disturbance was confirmed as the reason for failure of impulsive control.

By using some form of continuous-time control, however, transient amplification can be (essentially) eliminated and normal rhythm can be stabilized for fibers at least as long as 4 cm. Continuous-time feedback was computed as a piece-wise constant signal, with the number of sub-intervals ranging from 4 to 100 per pacing interval. Increasing the number of intervals improved the rate at which the disturbances about normal rhythm are suppressed, with the feedback current computed using the largest number of sub-intervals almost indistinguishable from a smooth optimal shape with the profile very similar to the shape of the adjoint eigenfunctions of the linearized evolution operator corresponding to the unstable modes.

The success of feedback control in suppressing the in-

stability of normal rhythm for all pacing rates and for Purkinje fibers of physiological dimensions (for human hearts) has important practical implications. The ability to control large tissue sizes with a single electrode has significant advantages in clinical applications where implanting a large number of electrodes increases the complexity of the procedure and the likelihood of complications. The next step in exploring the limits of feedback control is to test the proposed approach for models of two- and three-dimensional cardiac tissue.

ACKNOWLEDGMENTS

This material is partially based upon work supported by the National Science Foundation under Grants No. 1028133 (ROG) and 1341128 (FHF). A portion of this work (FHF) was also supported by the National Heart, Lung and Blood Institute of the National Institutes of Health, Award No. R01HL089271. The content is solely the responsibility of the authors, and does not necessarily represent the official views of the NIH.

REFERENCES

- ¹Hugh Calkins, Karl Heinz Kuck, Riccardo Cappato, Josep Brugada, A John Camm, Shih-Ann Chen, Harry J G Crijns, Ralph J Damiano, D Wyn Davies, John DiMarco, James Edgerton, Kenneth Ellenbogen, Michael D Ezekowitz, David E Haines, Michel Haissaguerre, Gerhard Hindricks, Yoshito Iesaka, Warren Jackman, Jose Jalife, Pierre Jais, Jonathan Kalman, David Keane, Young-Hoon Kim, Paulus Kirchhof, George Klein, Hans Kottkamp, Koichiro Kumagai, Bruce D Lindsay, Moussa Mansour, Francis E Marchlinski, Patrick M McCarthy, J Lluis Mont, Fred Morady, Koonlawee Nademanee, Hiroshi Nakagawa, Andrea Natale, Stanley Nattel, Douglas L Packer, Carlo Pappone, Eric Prystowsky, Antonio Raviele, Vivek Reddy, Jeremy N Ruskin, Richard J Shemin, Hsuan-Ming Tsao, and David Wilber, “2012 HRS/EHRA/ECAS Expert Consensus Statement on Catheter and Surgical Ablation of Atrial Fibrillation: recommendations for patient selection, procedural techniques, patient management and follow-up, definitions, endpoints, and research trial design..” *Europace* **14**, 528–606 (Apr. 2012).
- ²R H Clayton, O Bernus, E M Cherry, H Dierckx, F H Fenton, L Mirabella, A V Panfilov, F B Sachse, G Seemann, and H Zhang, “Models of cardiac tissue electrophysiology: progress, challenges and open questions..” *Progress in biophysics and molecular biology* **104**, 22–48 (Jan. 2011).
- ³Martin Fink, Steven A Niederer, Elizabeth M Cherry, Flavio H Fenton, Jussi T Koivumäki, Gunnar Seemann, Rüdiger Thul, Henggui Zhang, Frank B Sachse, Dan Beard, Edmund J Crampin, and Nicolas P Smith, “Cardiac cell modelling: observations from the heart of the cardiac physiome project..” *Progress in biophysics and molecular biology* **104**, 2–21 (Jan. 2011).
- ⁴Jorge M Davidenko, Arcady V. Pertsov, Remy Salomonsz, William Baxter, and José Jalife, “Stationary and drifting spiral waves of excitation in isolated muscle,” *Nature* **355**, 349–351 (Jan. 1992).
- ⁵R. A. Gray, A. M. Pertsov, and J. Jalife, “Spatial and temporal organization during cardiac fibrillation,” *Nature* **392**, 75–78 (1998).
- ⁶Stefan Luther, Flavio H Fenton, Bruce G Kornreich, Amgad Squires, Philip Bittihn, Daniel Hornung, Markus Zabel, James Flanders, Andrea Gladuli, Luis Campoy, Elizabeth M Cherry, Gisa Luther, Gerd Hasenfuss, Valentin I Krinsky, Alain Pumir, Robert F Gilmour, and Eberhard Bodenschatz, “Low-energy control of electrical turbulence in the heart..” *Nature* **475**, 235–9 (Jul. 2011).
- ⁷E. M. Cherry and F. H. Fenton, “Visualization of spiral and scroll waves in simulated and experimental cardiac tissue,” *New J. Phys.* **10**, 125016 (2008).
- ⁸J. M. Pastore, S. D. Girouard, K. R. Laurita, F. G. Akar, and D. S. Rosenbaum, “Mechanism linking T-wave alternans to the genesis of cardiac fibrillation,” *Circulation* **99**, 1385–1394 (1999).
- ⁹M. A. Watanabe, F. H. Fenton, S. J. Evans, H. M. Hastings, and A. Karma, “Mechanisms for discordant alternans,” *J. Cardiovasc. Electrophysiol.* **12**, 196–206 (2001).
- ¹⁰D. J. Christini, M. L. Riccio, C. A. Cuianu, J. J. Fox, A. Karma, and R. F. Gilmour, “Control of electrical alternans in canine cardiac Purkinje fibers,” *Phys. Rev. Lett.* **96**, 104101 (2006).
- ¹¹M. L. Koller, M. L. Riccio, and R. F. Gilmour Jr., “Dynamic restitution of action potential duration during electrical alternans and ventricular fibrillation,” *Am. J. Physiol.* **275**, H1635 (1998).
- ¹²E. M. Cherry and F. H. Fenton, “A tale of two dogs: Analyzing two models of canine ventricular electrophysiology,” *Am. J. Physiol. Heart Circ. Physiol.* **292**, H43–55 (2007).
- ¹³F. H. Fenton and E. M. Cherry, “Models of cardiac cell,” *Scholarpedia* **3**, 1868 (2008).
- ¹⁴D. Noble, “A modification of the Hodgkin-Huxley equations applicable to Purkinje fibre action and pace-maker potentials,” *J. Physiol.* **160**, 317–352 (1962).
- ¹⁵D. DiFrancesco and D. Noble, “A model of cardiac electrical activity incorporating ionic pumps and concentration changes,” *Philos. Trans. R. Soc. Lond. B Biol. Sci.* **307**, 353–398 (1985).
- ¹⁶O. V. Aslanidi, P. Stewart, M. R. Boyett, and H. Zhang, “Optimal velocity and safety of discontinuous conduction through the heterogeneous Purkinje-ventricular junction,” *Biophys. J.* **97**, 20–39 (2009).
- ¹⁷K. J. Sampson, V. Iyer, A. R. Marks, and R. S. Kass, “A computational model of purkinje fibre single cell electrophysiology: implications for the long qt syndrome,” *J. Physiol.* **588**, 2643–2655 (2010).
- ¹⁸F. H. Fenton and E. M. Cherry, “Minimal model for cardiac Purkinje fibers derived from experiments; a quantitative model for alternans,” (unpublished).
- ¹⁹K. Hall, D. J. Christini, M. Tremblay, J. J. Collins, L. Glass, and J. Billette, “Dynamic control of cardiac alternans,” *Phys. Rev. Lett.* **78**, 4518 (1997).
- ²⁰W.-J. Rappel, F. Fenton, and A. Karma, “Spatiotemporal control of wave instabilities in cardiac tissue,” *Phys. Rev. Lett.* **83**, 456–459 (1999).
- ²¹D. Chen, H. O. Wang, and W. Chin, “Suppressing cardiac alternans: analysis and control of a border-collision bifurcation in a cardiac conduction model,” in *Proc. IEEE Intl. Symposium on Circuits and Systems*, Vol. 3 (Monterey, CA, 1998) p. 635.
- ²²A. Garzón, R. O. Grigoriev, and F. H. Fenton, “Model-based control of cardiac alternans on a ring,” *Phys. Rev. E* **80**, 021932 (2009).
- ²³P. N. Jordan and D. J. Christini, “Adaptive diastolic interval control of cardiac action potential duration alternans,” *J. Cardiovasc. Electrophysiol.* **15**, 1177–1185 (2004).
- ²⁴S. Dubljevic, S.-F. Lin, and P. D. Christofides, “Studies of feedback control of cardiac alternans,” *Comp. Chem. Eng.* **32**, 2086 (2008).
- ²⁵S. Dubljevic, “Optimal boundary control of cardiac alternans,” *Int. J. Robust Nonlinear Control* **19**, 135 (2009).
- ²⁶B. Echebarria and A. Karma, “Instability and spatiotemporal dynamics of alternans in paced cardiac tissue,” *Phys. Rev. Lett.* **88**, 208101 (2002).
- ²⁷A. Garzón, R. O. Grigoriev, and F. H. Fenton, “Model-based control of cardiac alternans in Purkinje fibers,” *Phys. Rev. E* **84**, 041927 (2011).
- ²⁸R. O. Grigoriev and A. Handel, “Spectral theory for the failure

- of linear control in a nonlinear stochastic system,” *Phys. Rev. E* **66**, 065301(R) (2002).
- ²⁹A. Handel and R. O. Grigoriev, “Pattern selection and control via localized feedback,” *Phys. Rev. E* **72**, 066208 (2005).
- ³⁰A. Handel and R. O. Grigoriev, “Transient dynamics and nonlinear stability of spatially extended systems,” *Phys. Rev. E* **74**, 036302 (2006).
- ³¹M. F. Sheets, C. T. January, and H. A. Fozzard, “Isolation and characterization of single canine cardiac purkinje cells,” *Circ. Res.* **53**, 544–548 (1983).
- ³²I S Cohen, R T Falk, and R P Kline, “Voltage-clamp studies on the canine Purkinje strand..” *Proc. R. Soc. Lond. B* **217**, 215–36 (1982).
- ³³M. L. Pressler, V. Elharrar, and J. C. Bailey, “Effects of extracellular calcium ions, verapamil, and lanthanum on active and passive properties of canine cardiac purkinje fibers,” *Circ. Res.* **51**, 637–651 (1982).
- ³⁴Alessio Gizzi, Elizabeth M Cherry, Robert F Gilmour, Stefan Luther, Simonetta Filippi, and Flavio H Fenton, “Effects of pacing site and stimulation history on alternans dynamics and the development of complex spatiotemporal patterns in cardiac tissue..” *Frontiers in physiology* **4**, 71 (Jan. 2013).
- ³⁵D. A. Knoll and D. E. Keyes, “Jacobian-free Newton-Krylov methods: A survey of approaches and applications,” *J. Comp. Phys.* **193**, 357 (2004).
- ³⁶R. B. Lehoucq, D. C. Sorensen, and C. Yang, *ARPACK Users’ Guide: Solution of Large-Scale Eigenvalue Problems with Implicitly Restarted Arnoldi Methods* (SIAM Publications, Philadelphia, 1998).
- ³⁷Carolyn M. Berger, Xiaopeng Zhao, David G. Schaeffer, M. Dobrowolny, Wanda Krassowska, and Daniel J. Gauthier, “Period-doubling bifurcation to alternans in paced cardiac tissue: Crossover from smooth to border-collision characteristics,” *Phys. Rev. Lett.* **99**, 058101 (2007).
- ³⁸P. Dorato, C. T. Abdallah, and V. Cerone, *Linear-Quadratic Control* (Krieger Publishing Company, Melbourne, 2000).
- ³⁹Ivo Houtzager, “Discrete-time periodic Riccati equation solver for periodic LQ state-feedback design,” (2008), <http://www.mathworks.com/matlabcentral/fileexchange/21379-dpre>.
- ⁴⁰J. J. Hench and A. J. Laub, “Numerical solution of the discrete-time periodic riccati equation,” *IEEE Transactions on Automatic Control* **39**, 1197 (1994).